Nanoscale

Manipulating Phonon Polaritons in Low Loss ^{11}B enriched Hexagonal Boron Nitride with Polarization Control

Journal:	*Nanoscale*
Manuscript ID	NR-COM-02-2020-001067.R1
Article Type:	Communication
Date Submitted by the Author:	06-Mar-2020
Complete List of Authors:	Wang, Lu; Institute of Physics Chinese Academy of Sciences Key Laboratory of Optical Physics Chen, Runkun; Institute of Physics Chinese Academy of Sciences Key Laboratory of Optical Physics Xue, MengFei; Institute of Physics Chinese Academy of Sciences Key Laboratory of Optical Physics Liu, Song; Kansas State University, Department of Chemical Engineering Edgar, Jim; Kansas State University, Department of Chemical Engineering Chen, Jianing; Institute of Physics Chinese Academy of Sciences Key Laboratory of Optical Physics

COMMUNICATION

Manipulating Phonon Polaritons in Low Loss ^{11}B enriched Hexagonal Boron Nitride with Polarization Control

Received 00th January 20xx,
Accepted 00th January 20xx

DOI: 10.1039/x0xx00000x

Lu Wang,[a,b] Runkun Chen,[a,b] Mengfei Xue,[a,b] Song Liu,[c] James H. Edgar [c] and Jianing Chen *[a,b,d]

Abstract: Hexagonal boron nitride (hBN) supports two types of hyperbolic phonon polaritons (HPPs), whose properties of strong electromagnetic field confinement and low propagation loss[1] have been proposed for various applications in nanophotonics[2-4]. Conventionally, real-space imaging of HPPs by scattering-type scanning near-field optical microscopy (s-SNOM) with vertical polarization excitation contains both tip and edge launched polaritons modes, which leads to hybrid interference fringes. In this work, we symmetrically study the tip and edge excited HPPs in both boron nitride with the natural distribution of boron isotopes (Natural hBN) and ^{11}B isotope-enriched boron nitride (99.2% ^{11}B hBN). The intrinsic HPPs excited in 99.2% ^{11}B hBN exhibits a lower damping rate and longer propagation length than that in Natural hBN. We experimentally realize a tuning from a tip-dominated to an edge-dominated excited HPPs by rotating the polarization of incident light. The near-field electric field intensity (NEFI) of edge-excited HPPs E_{edge} and the angle β (between the hBN edge and the projective direction of the incident electric field on hBN plane) present a sine function relationship as $E_{edge} \propto |\sin \beta|$ under an *s*-polarized incident light. The NEFI of edge-excited HPPs in 99.2% ^{11}B hBN shows a 10% enhancement compared to Natural hBN under the same measurement conditons. Our findings demonstrate an effective approach to reducing phonon polaritons damping and manipulate phonon polaritons excitation in the hBN, which are beneficial for developing HPPs-based nanophotonic applications.

Introduction

Phonon polaritons (PP) are the coupled collective excitations of photon and phonon quasiparticles in crystals[3, 5-9]. PP are known for their remarkable properties such as strong field confinement, long propagation distance and low loss, which are advantageous for a wide range of applications in subdiffractional focusing[2, 10], optics[11, 12], and biosensing[13]. Hexagonal boron nitride is a representative Van der Waals (vdW) material, which exhibits hyperbolic dispersion in two Reststrahlen bands. In these two bands, the in-plane Re ε_t and out-of-plane Re ε_z dielectric permittivities along orthogonal crystal axes have opposite signs, which makes it possible to support hyperbolic phonon polaritons[14, 15]. In the lower band (760~820 cm^{-1}) the Re ε_z is negative, and the Re ε_t is positive, supporting type Ⅰ HPPs, and in the upper band (1365~1610 cm^{-1}) the signs of dielectric permittivities are opposite, supporting type Ⅱ HPPs[1, 3, 6, 11, 16-18]. Scattering-type scanning near-field optical microscopy (s-SNOM) is a powerful tool for studying phonon polaritons in real-space[19-22]. HPPs in boron nitride can be excited by both the metallic tip of the atomic force microscope (AFM) and the edges of hBN[6, 23-25]. HPPs excited by the AFM tip radiate outwards from the tip and gets reflected after reaching the edges or defects, and thus forms the interference fringes detected by the tip. HPPs excited by the edges of hBN propagate inward directly from the edges and get detected by the tip without interference. The interference-free edge-excited HPPs directly reflects the intrinsic properties of HPPs, which is more convenient for wavefront manipulation and applications in hBN photonic devices. Note a dielectric tip allows for imaging HPPs in the near-field without disturbing the tip-excited mode[26] in some circumstances. Nevertheless , the weak scattering signal is a general major obstacle for most polaritonic imaging and spectroscopic studies.

In this work, boron nitride with the natural distribution of boron isotopes (Natural hBN) and ^{11}B isotope-enriched boron nitride (99.2% ^{11}B hBN) were used to launch HPPs. To retain the enhanced scattering near field signal[27, 28], we used a metallic tip and changed the polarization of illuminated light to tune the excited HPPs fringes in hBN. As a result, we achieved near-field fringes dominated by tip-excited HPPs under *p*-polarized incident light, and near-field fringes dominated by edge-excited

[a] The Institute of Physics, Chinese Academy of Sciences, P.O. Box 603, Beijing, 100190, China. E-mail: jnchen@iphy.ac.cn.
[b] School of Physical Sciences, University of Chinese Academy of Sciences, Beijing 100049, China
[c] Tim Taylor Department of Chemical Engineering, Kansas State University, Manhattan, KS 66506 U.S.A.
[d] Songshan Lake Materials Laboratory Dongguan, 523808 Guangdong, China
†Electronic Supplementary Information (ESI) available: [Materials and Methods and Supplemental experiments and simulations.]. See DOI: 10.1039/x0xx00000x

HPPs under *s*-polarized incident light. Under the *s*-polarized incident light, the NEFI of edge-excited HPPs depends on the polarized angle β (Fig. 1a), which is between the direction of the electric field of incident light and the hBN edge. Combined with numerical simulation, we reveal that HPPs can be launched only by the component of the electric field vertical to the flake edge. Therefore, the NEFI of edge-excited HPPs has an angularly dependent relation with sinβ. This angular dependence leads to a distinct modulation of fringes formed by HPPs in the hBN flake, and we show that these effects can be found both in naturally abundant and ^{11}B isotope-enriched hBN flakes. By decomposing the hybrid fringe profiles of HPPs, we show that the intrinsic HPPs in isotopically enriched hBN exhibits a lower damping rate and thus travel longer. Moreover, the NEFI of edge-excited HPPs in 99.2% ^{11}B hBN is 10% higher than that in Natural hBN, which suggests a stronger interaction with light.

Results and discussion

Both naturally abundant and isotope enriched hBN slabs were obtained by mechanical exfoliation. The surfaces of these hBN slabs are atomically flat with thickness of about 80 nm (shown in Fig. S1). Raman spectroscopy was conducted to characterize these hBN slabs (Fig. S2). The isotope-enriched hBN exhibits a red shift of Raman peak from 1365.6 cm^{-1} to 1356 cm^{-1}, which suggests a 99.2% ^{11}B enrichment in this hBN sample[29]. An s-SNOM equipped with a monochromatic quantum cascade laser (QCLs) with spectral range $\nu = 1500\sim1600\ cm^{-1}$ was used to image the near-field fringes formed by the propagating type II HPPs in hBN in real space. The experimental configuration is shown in Fig. 1a, a *p*-polarized (*s*-polarized) laser is focused on the metallic tip and the hBN, and thus excites HPPs in hBN. For a *p*-polarized incident light at 1502 cm^{-1}, the near-field images of hBN are shown in Fig. 1b and 1c, where the fringes are parallel to the hBN edge (white dashed line) and extend to the interior part of the hBN. The amplitude of the hybrid fringes represents the electric field intensity in the near-filed of the hybrid HPPs. The amplitude line profiles extracted from the yellow dashed line in Fig. 1b and 1c are plotted in Fig. 1d, which

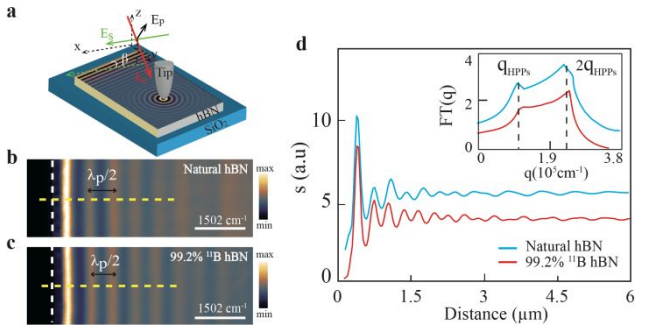

Figure 1. Experimental schematic and near field imaging of HPPs. (a) Schematic of near field imaging of HPPs. (b), (c) Real-space imaging of HPPs in hBN. The scale bar is 2 um. (d) Amplitude line profiles taken along the yellow dashed line in Fig. 1(b) and 1(c). Inset: The Fourier transform spectra of the corresponding line profiles.

show a hybrid interference fringe. The Fourier transform spectra (FT) (Fig. 1d inset) displays two peaks, indicating the existence of both tip and edge excited HPPs. The intensity contrast in FT also suggests a tip excited HPPs dominates the fringes.

A broad-band Fourier transform infrared nanospectroscopy (Nano-FTIR) is conducted to investigate the HPPs in hBN at a frequency range from 1400 cm^{-1} to 1500 cm^{-1}. There is no resonance for SiO_2 substrate in the spectral range $\nu = 1400\sim1600\ cm^{-1}$, therefore the spectral response of the naturally abundant hBN and isotope-enriched hBN can be clearly presented. Each point of the scanning line perpendicular to the hBN edge in the broad-band Nano-FTIR spectra composes a two-dimensional spectra distribution maps $s = s(L,\nu)$ as shown in Fig. 2a and 2b. The amplitude of the color scale in Fig. 2a and 2b indicates the intensity of the Nano-FTIR spectra taken along the horizontal axis. At a fixed frequency, a series of peaks along the scanning line appear, and the interval of adjacent bright peaks is the same, which is equal to half of the HPPs wavelength ($\lambda_p/2$) due to the interference. Through the Nano-FTIR spectra, a clear additional two interference peaks (marked as red triangles and white stars) appear in the 99.2% ^{11}B hBN, which suggests a lower damping rate (longer propagation distance). The experimental dispersion relationship $q = q(\nu)$

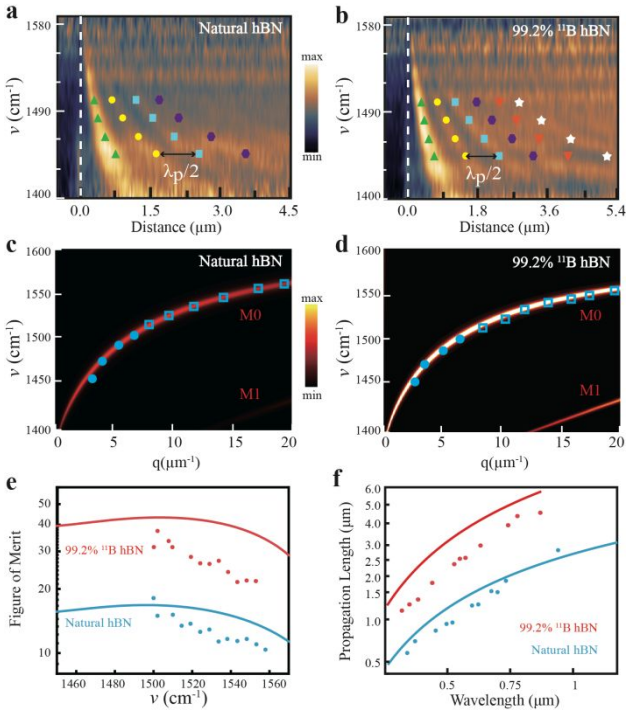

Figure 2. The Nano-FTIR spectra, dispersion of HPPs in hBN. (a), (b) Line scan nano-FTIR spectra taken along the direction perpendicular to the hBN edge on two kinds of hBN crystal. (c), (d) Dispersion relation of phonon polaritons in Natural and 99.2% ^{11}B hBN, the blue boxes and dots are experimental data extracted from monochromatic imaging and the Nano-FTIR result respectively. (e) The figure of merit as a function of incident frequency. (f) The HPPs propagation lengths as a function of HPPs wavelength.

can be extracted from the monochromatic near field imaging (blue boxes) and Nano-FTIR (blue dots) experiments as shown in Fig. 2c and 2d. For comparison, the imaginary part of reflectivity of Natural hBN with thickness of 80 nm and 99.2% ^{11}B hBN with thickness of 84 nm on a SiO_2 substrate are calculated, which represents the theoretical dispersion of HPPs in hBN. It shows a good agreement between the experimental data and the calculated principal branch of hyperbolic

polaritons (M0). The higher intensity of the false-color (M0, M1) indicates a stronger optical losses[29] of incident light in the 99.2% ^{11}B hBN samples, which suggests a stronger interaction between light and the 99.2% ^{11}B hBN.

To quantitatively analyze the damping of the Natural hBN and the 99.2% ^{11}B hBN, the hybrid fringes (Fig. 1d) composed of tip-excited mode[6, 8, 10, 16] (period $\lambda_p/2$) and edge-excited mode[24] (period λ_p) at different frequencies are fitted with equation:

$$E_{total} = E_1 + E_{tip}(x) + E_{edge}(x) = E_1(1 + b * e^{i2qx}/\sqrt{x} + c * e^{iqx}) \quad (1)$$

Where the first term E_1 indicates the field strength of the HPPs inside of hBN away from the edge, which is related to the power of the incident laser; the second term $E_{tip}(x)$ describes the tip-excited HPPs with a geometric damping factor[1, 26] $1/\sqrt{x}$ of a cylinder wave; the third term represents the edge-excited HPPs. The parameter $q = \mathrm{Re}(q) + i * \mathrm{Im}(q)$ is the wave vector of HPPs, and another two parameters b and c represent the relative strength of tip-excited mode and edge-excited mode respectively. Note that the first peak in the line profile is excluded from fitting due to the complex physical origin[1]. Therefore, the intrinsic propagation figure of merit[29] (FOM) $Q = 1/\gamma$(the damping rate$\gamma = \mathrm{Im}(q)/\mathrm{Re}(q)$) and propagation length[1] $L = 1/\mathrm{Im}(q)$ can be extracted directly from the hybrid fringes line profiles. There is a twofold improvement in FOM and propagation length in the isotopically 99.2% ^{11}B hBN from both experimental (dots) and numerical calculation (solid lines) results in Fig. 2e and 2f. However, the FOM and propagation length in the 99.2% ^{11}B hBN deviate from the experiment result, which we attribute to a greater actual phonon damping in our sample than the previous reports[29].

Theoretically, the tip-light coupling efficiency is related to the polarization of incident light[22]. Based on this consideration, we rotate the polarization direction of the incident laser from the vertical direction (*p*-polarized) to the horizontal direction (*s*-polarized) in the hBN plane. In this polarization configuration, the direction of the *s*-polarized electric field is perpendicular to the long axis of tip that can significantly reduce polarization[30] of the metallic tip. Fig. 3a-d show the experimental near-field images of Natural and 99.2% ^{11}B hBN with different polarized angle β under an *s*-polarized laser. As shown in Fig. 3a (Fig. 3c), the distance of the main fringes in Natural hBN (99.2% ^{11}B hBN) is about 880nm (820nm), which is approximately equal to theoretical dispersion result λ_p=890nm (λ_p=860nm) at 1502 cm^{-1}, and the interval of the first four bright fringes is about 435nm (418nm), which is approximately equal to $\lambda_p/2$. Compared with the *p*-polarized situation (Fig. 1d), the HPPs excited by the *s*-polarized light is dominated by the edge-excited mode, which indicates that the hBN edge is able to directly launch HPPs, and the fringes intensity is strong enough to be observed directly by suppressing the tip-excited mode. When the angle β is set to 2° as shown in Fig. 3b and 3d, the fringe spacing is only half of HPPs wavelength, which indicates that the edge-excited mode almost disappears while the tip-excited mode is reserved.

To further understand our experimental results, we carried out a numerical simulation using the three-dimensional wave optical module in COMSOL software. In the simulation, an *s*-polarized plane wave was set to replace the laser to illuminate the edge of hBN. The simulated vertical component of electric field[31] E_z is used to compare with the experimental edge-excited HPPs corresponding to the same angle β are shown in Fig. 3e-h. Clearly, the NEFI of HPPs decrease with reducing polarized angle β. When the polarized angle β=2°, the NEFI of edge-excited HPPs is almost negligible and becomes zero when the polarized

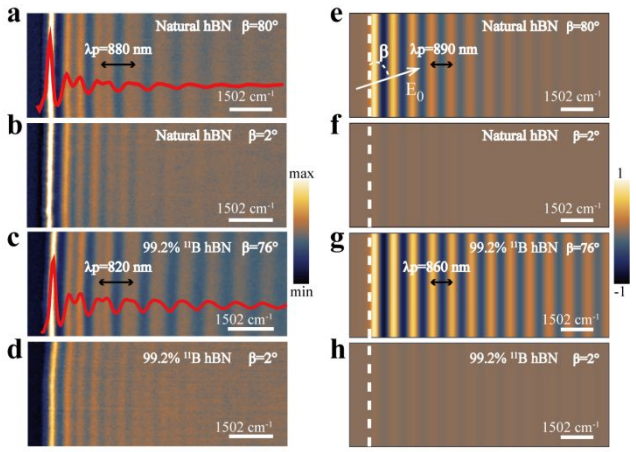

Figure 3. Near-field nano-imaging and numerical simulation results of HPPs excited by the hBN edge. (a) – (d) Near-field amplitude images of Natural hBN and isotope-enriched hBN with *s*-polarization at different β. The red line is the line profile taken perpendicular to the hBN edge, representing the near-field amplitude as a function of the distance from the hBN edge. (e) – (h) The simulation results of vertical component of electric field E_z in Natural hBN and 99.2% ^{11}B hBN with *s*-polarization at different β. IR frequency: 1502 cm^{-1}, the scale bar is 1.5 um.

angle equal to 0° (see in Fig. S6). This implies that the fringes in Fig. 3b and 3d are the weak tip-excited HPPs due to the residual polarization of the metallic tip. In the simulation, the s-pol light only excites the edge excited HPPs. However, the measured images with s-pol incident light unavoidably contain both the edge excited and the weak tip excited HPPs, which is the cause of deviation between the experimental and calculated results. The NEFI of HPPs excited by the edge is related to the polarized angle of the incident light. A quantitative analysis of the excitation and damping of edge-excited HPPs will be discussed in detail below.

As shown in Fig. 4a-d, the experimental amplitude profiles of edge-excited HPPs at different polarized angle β for both Natural and 99.2% ^{11}B hBN are well fitted with equation (1). The overall oscillation curve is superimposed by the edge-excited (blue curve) and the tip-excited (green curve) HPPs. The curves are vertically separated for better demonstration. The damping rate $\gamma = \mathrm{Im}(q)/\mathrm{Re}(q)$ is 0.065 for Natural hBN and 0.025 for 99.2% ^{11}B hBN respectively for all polarized angle β, which indicates that the damping ratio of HPPs excited in Natural and 99.2% ^{11}B hBN is independent of the polarized angle β. Apart from that, HPPs launched in 99.2% ^{11}B hBN (no matter the p or s polarized and the tip or edge excited HPPs) exhibits a lower

intrinsic damping rate because the isotopically pure material effectively reduce the scattering caused by isotopic disorder in the crystal[29].

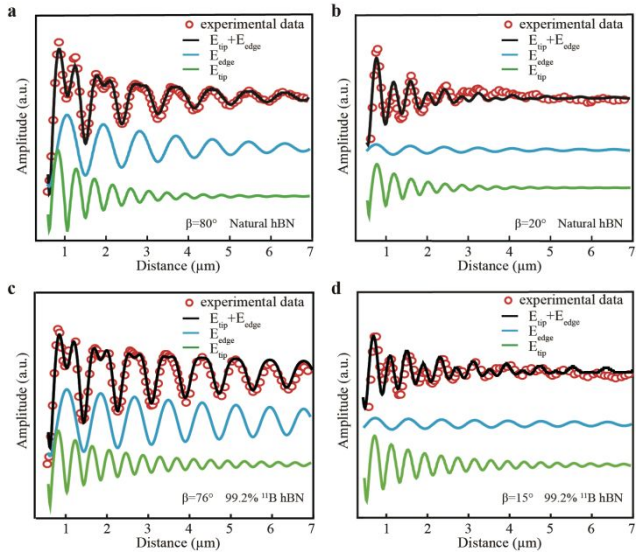

Figure 4. Theoretical fitting of the experimental amplitude profiles. (a), (b) Theoretical fitting of the extracted profiles in Natural hBN at different β. (c), (d) Theoretical fitting of the extracted profiles in 99.2% ^{11}B hBN at different β. The red rings are the experimental results, and the black line represents the theoretical fitting, including the edge-excited mode (blue line) and the tip-excited mode (green line). IR frequency: 1502 cm^{-1}.

Note that the NEFI of edge-excited HPPs is related to the polarized angle β. As shown in Fig. 5 the angular dependence of normalized NEFI of HPPs based on experiment and simulation results are plotted (The intensity of edge-excited HPPs at a polarized angle 90° in 99.2% ^{11}B hBN is used for normalization). The blue boxes (line) and red rings (line) in Fig. 5a are the experimental (simulation) results for Natural and 99.2% ^{11}B hBN respectively. The normalized NEFI of edge-excited HPPs gradually increases as the polarization angle changes from 0° to 90°, which matches the simulation results plotted as the solid lines. The angular dependence of the edge-excited mode HPPs excitation efficiency can be theoretically fitted well with a sine function $E_{edge} \propto |\sin\beta|$, which exactly coincides with the simulation results and previous reported[26] (the theoretical fitting with the simulation results is shown in Fig. S7). The NEFI of HPPs in 99.2% ^{11}B hBN is stronger than the intensity of HPPs in Natural hBN at any polarized angle β, and it shows a 10% enhancement, which suggests a stronger coupling between incident light and edge-excited HPPs in the 99.2% ^{11}B hBN. We calculate the maximum imaginary part of the reflectivity r_p of Natural hBN and 99.2% ^{11}B hBN with the same thickness of 80 nm on a SiO_2 substrate in Fig. 5b. Clearly, the maximum imaginary part of the reflectivity (corresponding to the optical losses of the incident light) in the 99.2% ^{11}B hBN is stronger than that in Natural hBN, which indicates the 99.2% ^{11}B hBN has more significant application potential in field enhancement and enhanced spectroscopy.

Conclusions

Our results show that the electromagnetic wave in free space illuminated on the edge of hBN is able to launch the HPPs propagating inward from the hBN edge. By changing the *p*-polarized incident light to an *s*-polarized light, we demonstrate a way to suppress the tip-excited HPPs in hBN effectively. We found the intrinsic property of HPPs in 99.2% ^{11}B hBN exhibits a lower damping rate and longer propagation length. The NEFI of

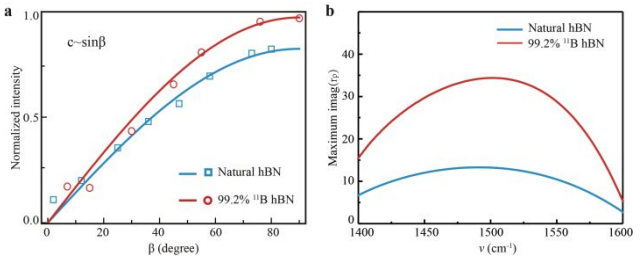

Figure 5. Angular dependence of the excitation of HPPs. (a) Angularly dependent edge excitation normalized NEFI of HPPs in Natural hBN and 99.2% ^{11}B hBN. The blue boxes and red rings are the experimental data. The blue and red solid lines show the simulation results. IR frequency: 1502 cm^{-1}. (b) The maximum imaginary part of reflectivity r_p of Natural hBN and 99.2% ^{11}B hBN with the same thickness of 80 nm on a SiO_2 substrate.

the edge-excited HPPs is angularly dependent with the angle between the electric field of incident light and the direction along the hBN edge as $E_{edge} \propto |\sin\beta|$. The intensity of edge-excited HPPs in 99.2% ^{11}B hBN shows a 10% enhancement than that in Natural hBN. Our results offer an effective way to realize a low loss and tunable surface electric field distribution by HPPs in isotopically hBN. Our findings are beneficial for promoting the development of HPPs based nanophotonic applications in the future.

Acknowledgements

This work was supported by the National Key Research and Development Program of China (2016YFA0203500), National Natural Science Foundation of China (Grant No.11874407), and Strategic Priority Research Program of Chinese Academy of Science (Grant No. XDB 30000000). Support for hBN crystal growth from the Materials Engineering and Processing program of the National Science Foundation, Award Number CMMI 1538127, and the II–VI Foundation is greatly appreciated.

Conflicts of interest

The authors state no potential conflict of interest.

References

1. E. Yoxall, M. Schnell, A. Y. Nikitin, O. Txoperena, A. Woessner, M. B. Lundeberg, F. Casanova, L. E. Hueso, F. H. L. Koppens and R. Hillenbrand, *Nat Photonics*, 2015, **9**, 674-+.
2. P. N. Li, M. Lewin, A. V. Kretinin, J. D. Caldwell, K. S. Novoselov, T. Taniguchi, K. Watanabe, F. Gaussmann and T. Taubner, *Nat Commun*, 2015, **6**.
3. J. D. Caldwell, A. V. Kretinin, Y. G. Chen, V. Giannini, M. M. Fogler, Y. Francescato, C. T. Ellis, J. G. Tischler, C. R. Woods, A. J. Giles, M. Hong, K. Watanabe, T. Taniguchi, S. A. Maier and K. S. Novoselov, *Nat Commun*, 2014, **5**.

4. A. J. Giles, S. Y. Dai, O. J. Glembocki, A. V. Kretinin, Z. Y. Sun, C. T. Ellis, J. G. Tischler, T. Taniguchi, K. Watanabe, M. M. Fogler, K. S. Novoselov, D. N. Basov and J. D. Caldwell, *Nano Lett*, 2016, **16**, 3858-3865.
5. A. J. Huber, B. Deutsch, L. Novotny and R. Hillenbrand, *Appl Phys Lett*, 2008, **92**.
6. S. Dai, Z. Fei, Q. Ma, A. S. Rodin, M. Wagner, A. S. McLeod, M. K. Liu, W. Gannett, W. Regan, K. Watanabe, T. Taniguchi, M. Thiemens, G. Dominguez, A. H. C. Neto, A. Zettl, F. Keilmann, P. Jarillo-Herrero, M. M. Fogler and D. N. Basov, *Science*, 2014, **343**, 1125-1129.
7. R. Hillenbrand, T. Taubner and F. Keilmann, *Nature*, 2002, **418**, 159-162.
8. X. J. G. Xu, B. G. Ghamsari, J. H. Jiang, L. Gilburd, G. O. Andreev, C. Y. Zhi, Y. Bando, D. Golberg, P. Berini and G. C. Walker, *Nat Commun*, 2014, **5**.
9. Z. Jacob, *Nat Mater*, 2014, **13**, 1081-1083.
10. S. Dai, Q. Ma, T. Andersen, A. S. Mcleod, Z. Fei, M. K. Liu, M. Wagner, K. Watanabe, T. Taniguchi, M. Thiemens, F. Keilmann, P. Jarillo-Herrero, M. M. Fogler and D. N. Basov, *Nat Commun*, 2015, **6**.
11. Y. Y. Jiang, X. Lin, T. Low, B. L. Zhang and H. S. Chen, *Laser Photonics Rev*, 2018, **12**.
12. X. Lin, Y. Yang, N. Rivera, J. J. Lopez, Y. C. Shen, I. Kaminer, H. S. Chen, B. L. Zhang, J. D. Joannopoulos and M. Soljacic, *P Natl Acad Sci USA*, 2017, **114**, 6717-6721.
13. M. Autore, P. N. Li, I. Dolado, F. J. Alfaro-Mozaz, R. Esteban, A. Atxabal, F. Casanova, L. E. Hueso, P. Alonso-Gonzalez, J. Aizpurua, A. Y. Nikitin, S. Velez and R. Hillenbrand, *Light-Sci Appl*, 2018, **7**.
14. S. A. Biehs, M. Tschikin and P. Ben-Abdallah, *Phys Rev Lett*, 2012, **109**.
15. A. Poddubny, I. Iorsh, P. Belov and Y. Kivshar, *Nat Photonics*, 2013, **7**, 948-957.
16. Z. W. Shi, H. A. Bechtel, S. Berweger, Y. H. Sun, B. Zeng, C. H. Jin, H. Chang, M. C. Martin, M. B. Raschke and F. Wang, *Acs Photonics*, 2015, **2**, 790-796.
17. S. Y. Dai, M. Tymchenko, Y. F. Yang, Q. Ma, M. Pita-Vidal, K. Watanabe, T. Taniguchi, P. Jarillo-Herrero, M. M. Fogler, A. Alu and D. N. Basov, *Adv Mater*, 2018, **30**.
18. P. Li, I. Dolado, F. J. Alfaro-Mozaz, A. Y. Nikitin, F. Casanova, L. E. Hueso, S. Velez and R. Hillenbrand, *Nano Lett*, 2017, **17**, 228-235.
19. Z. Fei, A. S. Rodin, G. O. Andreev, W. Bao, A. S. McLeod, M. Wagner, L. M. Zhang, Z. Zhao, M. Thiemens, G. Dominguez, M. M. Fogler, A. H. Castro Neto, C. N. Lau, F. Keilmann and D. N. Basov, *Nature*, 2012, **487**, 82-85.
20. J. N. Chen, M. Badioli, P. Alonso-Gonzalez, S. Thongrattanasiri, F. Huth, J. Osmond, M. Spasenovic, A. Centeno, A. Pesquera, P. Godignon, A. Z. Elorza, N. Camara, F. J. G. de Abajo, R. Hillenbrand and F. H. L. Koppens, *Nature*, 2012, **487**, 77-81.
21. Z. Fei, A. S. Rodin, W. Gannett, S. Dai, W. Regan, M. Wagner, M. K. Liu, A. S. McLeod, G. Dominguez, M. Thiemens, A. H. C. Neto, F. Keilmann, A. Zettl, R. Hillenbrand, M. M. Fogler and D. N. Basov, *Nat Nanotechnol*, 2013, **8**, 821-825.
22. P. Alonso-Gonzalez, A. Y. Nikitin, F. Golmar, A. Centeno, A. Pesquera, S. Velez, J. Chen, G. Navickaite, F. Koppens, A. Zurutuza, F. Casanova, L. E. Hueso and R. Hillenbrand, *Science*, 2014, **344**, 1369-1373.
23. V. W. Brar, M. S. Jang, M. Sherrott, S. Kim, J. J. Lopez, L. B. Kim, M. Choi and H. Atwater, *Nano Lett*, 2014, **14**, 3876-3880.
24. S. Y. Dai, Q. Ma, Y. F. Yang, J. Rosenfeld, M. D. Goldflam, A. McLeod, Z. Y. Sun, T. I. Andersen, Z. Fei, M. K. Liu, Y. M. Shoa, K. Watanabe, T. Taniguchi, M. Thiemens, F. Keilmann, P. Jarillo-Herrero, M. M. Fogler and D. N. Basov, *Nano Lett*, 2017, **17**, 5285-5290.
25. J. Duan, R. Chen, J. Li, K. Jin, Z. Sun and J. Chen, 2017, **29**, 1702494.
26. G. Cheng, D. Wang, S. Dai, X. Fan, F. Wu, X. Li and C. Zeng, *Nanoscale*, 2018, **10**, 16314-16320.
27. A. García-Etxarri, I. Romero, F. J. García de Abajo, R. Hillenbrand and J. Aizpurua, *Physical Review B*, 2009, **79**, 125439.
28. J. Duan, Y. Li, Y. Zhou, Y. Cheng and J. Chen, *Advances in Physics: X*, 2019, **4**, 1593051.
29. A. J. Giles, S. Y. Dai, I. Vurgaftman, T. H. Man, S. Liu, L. Lindsay, C. T. Ellis, N. Assefa, I. Chatzakis, T. L. Reinecke, J. G. Tischler, M. M. Fogler, J. H. Edgar, D. N. Basov and J. D. Caldwell, *Nat Mater*, 2018, **17**, 134-+.
30. R. E. Larsen and H. J. J. o. C. P. Metiu, 2001, **114**, 6851-6860.
31. F. J. Alfaromozaz, P. Alonsogonzalez, S. Velez, I. Dolado, M. Autore, S. Mastel, F. Casanova, L. E. Hueso, P. Li and A. Y. Nikitin, *Nature Communications*, 2017, **8**, 15624-15624.

Manipulating Phonon Polaritons in Low Loss ^{11}B enriched Hexagonal Boron Nitride with Polarization Control

A table of contents entry

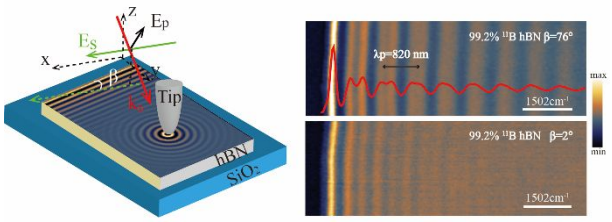

An effective approach to reducing phonon polaritons damping and manipulating phonon polaritons excitation in the hBN via polarization control